Serum-borne bioactivity caused by pulmonary multiwalled carbon nanotubes induces neuroinflammation via blood–brain barrier impairment

Mario J. Aragon[a], Lauren Topper[a], Christina R. Tyler[a], Bethany Sanchez[a], Katherine Zychowski[a], Tamara Young[a], Guy Herbert[a], Pamela Hall[a], Aaron Erdely[b], Tracy Eye[b], Lindsey Bishop[b], Samantha A. Saunders[c], Pretal P. Muldoon[c], Andrew K. Ottens[c,1], and Matthew J. Campen[a,1]

[a]Department of Pharmaceutical Sciences, College of Pharmacy, University of New Mexico, Albuquerque, NM 87131; [b]Pathology and Physiology Research Branch, National Institute for Occupational Safety and Health, Morgantown, WV 26505; and [c]Department of Anatomy and Neurobiology, School of Medicine, Virginia Commonwealth University, Richmond, VA 23298

Edited by Lawrence Steinman, Stanford University School of Medicine, Stanford, CA, and approved January 20, 2017 (received for review September 26, 2016)

Pulmonary exposure to multiwalled carbon nanotubes (MWCNTs) causes indirect systemic inflammation through unknown pathways. MWCNTs translocate only minimally from the lungs into the systemic circulation, suggesting that extrapulmonary toxicity may be caused indirectly by lung-derived factors entering the circulation. To assess a role for MWCNT-induced circulating factors in driving neuroinflammatory outcomes, mice were acutely exposed to MWCNTs (10 or 40 μg/mouse) via oropharyngeal aspiration. At 4 h after MWCNT exposure, broad disruption of the blood-brain barrier (BBB) was observed across the capillary bed with the small molecule fluorescein, concomitant with reactive astrocytosis. However, pronounced BBB permeation was noted, with frank albumin leakage around larger vessels (>10 μm), overlain by a dose-dependent astroglial scar-like formation and recruitment of phagocytic microglia. As affirmed by elevated inflammatory marker transcription, MWCNT-induced BBB disruption and neuroinflammation were abrogated by pretreatment with the rho kinase inhibitor fasudil. Serum from MWCNT-exposed mice induced expression of adhesion molecules in primary murine cerebrovascular endothelial cells and, in a wound-healing in vitro assay, impaired cell motility and cytokinesis. Serum thrombospondin-1 level was significantly increased after MWCNT exposure, and mice lacking the endogenous receptor CD36 were protected from the neuroinflammatory and BBB permeability effects of MWCNTs. In conclusion, acute pulmonary exposure to MWCNTs causes neuroinflammatory responses that are dependent on the disruption of BBB integrity.

nanoparticle | blood-brain barrier | microglia | thrombospondin-1 | multiwalled carbon nanotube

Environmental and occupational exposures to respirable toxicants are associated with neurodevelopmental and neurodegenerative outcomes (1–3). An influence of inhaled environmental stressors on the integrity of the blood-brain barrier (BBB) has been identified (4). BBB deficits are common to various pathologies and linked to phenotypic changes in microglial and astrocyte populations, which may detract from normal neurosupportive function essential to learning, memory, and neuroplasticity (5–7). The mechanism by which inhaled particulates may adversely impact the neurovascular unit and ultimately lead to neuroinflammatory outcomes remains unclear.

A subgroup of respirable particulate matter (PM), engineered nanoparticles, includes multiwalled carbon nanotubes (MWCNTs), which are being increasingly used in industry owing to their range of unique properties (8, 9). Inhalation of MWCNTs induces lung inflammation, as indicated by infiltration of inflammatory cells from the periphery, increased lung permeability, and fibrosis (10, 11). Despite their very limited ability to translocate beyond the lung (12), MWCNTs have been shown to induce extrapulmonary toxicity through as-yet unknown pathways (13–15). Pulmonary interactions with inhaled pollutants, including MWCNTs, can generate secondary bioactive factors that spill over into the systemic circulation and are distributed throughout the body (15–17). One consequence of these circulating factors is activation of the endothelium, characterized by the expression of adhesion molecules and recruitment/activation of circulating inflammatory cells (18). The nature and outcome of these effects are dependent on the vascular bed in which the inflammation occurs and can include systemic or cerebrovascular vessels.

Cerebrovascular inflammation increases permeability of the BBB (19), a specialized structure composed of astrocytes, pericytes, and endothelial cells (20). Under normal conditions, the BBB prevents passage of undesired molecules from the bloodstream into the central nervous system; however, under inflammatory conditions, the tight junctions between the endothelial cells can become destabilized, resulting in a leaky BBB and allowing peripheral inflammatory molecules to invade and activate neuroglial cells, specifically microglia (21) and astrocytes. Oppenheim et al. (22) found that inhalation of vehicle emissions increased BBB permeability, and also increased levels of inducible nitric oxide synthase and IL-1β in the parenchyma. Neuroinflammation has been demonstrated in rodent models exposed to PM or gaseous pollutants (23, 24); however, a mechanistic link between neuroinflammation and BBB permeability has not been established, and potential intermediate drivers of such effects remain unclear.

Significance

Inhaled particulates, such as multiwalled carbon nanotubes, can induce neuroinflammatory outcomes. The present study shows that acute neuroinflammation is dependent on the impairment of blood-brain barrier function. Pharmacologic restoration of blood-brain barrier integrity prevented the neuroinflammatory responses to pulmonary multiwalled carbon nanotube exposure. Circulating factors, including possibly thrombospondin-1, recapitulate inflammatory responses in cultured cerebrovascular endothelial cells, suggesting a mechanism for indirect systemic effects of inhaled nanoparticles.

Author contributions: M.J.A., A.E., A.K.O., and M.J.C. designed research; M.J.A., L.T., C.R.T., B.S., K.Z., T.Y., G.H., A.E., T.E., L.B., S.A.S., P.P.M., A.K.O., and M.J.C. performed research; P.H. contributed new reagents/analytic tools; M.J.A., L.T., C.R.T., B.S., K.Z., T.Y., G.H., T.E., L.B., S.A.S., P.P.M., A.K.O., and M.J.C. analyzed data; and M.J.A., C.R.T., P.H., A.E., A.K.O., and M.J.C. wrote the paper.

The authors declare no conflict of interest.

This article is a PNAS Direct Submission.

Freely available online through the PNAS open access option.

[1]To whom correspondence may be addressed. Email: akottens@vcu.edu or mcampen@salud.unm.edu.

This article contains supporting information online at www.pnas.org/lookup/suppl/doi:10.1073/pnas.1616070114/-/DCSupplemental.

We hypothesized that neuroinflammation arises after MWCNT exposure, owing at least in part to increased BBB permeability caused by circulating thrombospondin-1 (TSP-1). In this study, we demonstrate that MWCNT exposure induces the generation of circulating bioactive factors, leading to activation of the cerebrovasculature and inflammatory cells, as well as increased BBB permeability.

Results

Pulmonary Delivery of MWCNTs Drives Lung and Systemic Transcriptional Responses. Representative transmission and scanning electron microscopy images of the MWCNTs demonstrate the relative size and adequacy of dispersion (Fig. S1*A*). More thorough descriptions of the formulation and delivery methodologies for this material have been published previously (25). Following pulmonary exposure to 10 and 40 μg of MWCNTs, multiple markers of inflammation were significantly increased in the lungs, including systemic proinflammatory markers interleukin 6 (*Il6*) and C-C motif chemokine ligand 2 (*Ccl2*), as well as C-X-C motif chemokine ligand 2 (*Cxcl2*) (Fig. S1*B*). These effects persisted at 24 h in a primarily dose-dependent manner. In addition, MWCNT aspiration significantly induced liver enzyme gene expression, indicative of an acute inflammatory phase response that is systemic in nature (Fig. S1*C*). All responses were dose-dependent, with the 40 μg dose eliciting a particularly strong response. For remaining studies, we used the lower dose (10 μg) and focused on the 4 h time point to examine the earliest events at the lowest dose.

Evidence of Broad Cerebrovascular BBB Disruption and Glial Reactivity Following MWCNT Exposure. To test BBB integrity, we injected mice systemically with sodium fluorescein at 3 h after MWCNT exposure (i.e., 1 h before euthanasia). In cryosections of frontal cortex from control mice, fluorescein was not readily evident (Fig. 1*A*); however, in MWCNT-exposed mice, fluorescein was clearly present in close association with platelet endothelial cell adhesion molecule (PECAM)-stained cerebral capillaries, indicative of initial penetration through the cerebral wall (Fig. 1*B*). Immunohistochemistry analysis of the cerebellum and hippocampus in mice at 4 h after MWCNT exposure also revealed elevated glial fibrillary acidic protein (GFAP) staining density, indicative of reactive astrocytes, compared with dispersion medium (DM)-exposed control mice (Fig. 1 *C*–*H*).

Dose-Dependent MWCNT-Induced BBB Disruption and Neuroinflammation Around Larger Cerebrovasculature. To further assess the extent of MWCNT-induced BBB permeation, mouse brains were stained for extravascular albumin. Using the large molecule albumin to stain for a more pronounced compromise of the BBB, our study of the neurovascular unit became focused on larger-diameter vessels (>10-μm diameter), such as penetrating arterioles, that feed the microvasculature. In DM control mice, albumin-positive staining was not readily evident, with limited amounts found in close association with zonula occludens 1 (ZO1)-stained vessels, consistent with residual albumin following perfusion (Fig. 2*A*). Vessels in DM control brains exhibited the expected GFAP staining of astrocytic endfeet close to the vascular wall and typical IBA1 staining of a sentinel microglial cell toward one side; however, at 4 h after mice were exposed to MWCNTs at either dose, robust extravascular albumin staining was observed selectively accumulated around larger (>10-μm diameter) cerebrovasculature (Fig. 2*A*). Furthermore, vessels exhibiting this extravascular albumin halo were also enveloped by a dense accumulation of GFAP-stained astrocytes and ionized calcium-binding adapter molecule 1 (IBA1)-stained microglia, both with morphology indicative of activation following MWCNT exposure. Assessed over a population of similar-sized vessels (mean, 22.7 ± 4.9-μm diameter), the extent of glial ensheathment was dose-dependent, with the boundaries of reactive astrocytes and microglial extending 35.2% and 76.4% further, respectively, into the neuropil from the vessel wall in mice given 40 μg rather than 10 μg of MWCNTs (Fig. 2*B*). Glial activation was not noted broadly throughout the brain (Fig. S2), highlighting a selective response at the neurovascular unit.

Evidence for Differential Glial Functions in Reactivity to MWCNT-Induced BBB Disruption. The observation of astrocytic and microglial reactivity in close proximity to leaking vessels raised questions as to the respective functions of these cells. Optical sectioning revealed the accumulation of reactive astrocytes in a tight glial scar-like network distinct from the intermittent array of processes surrounding DM control vessels (GFAP staining; Fig. 2*C*). Furthermore, reactive astrocytic processes were seen to completely envelop capillary branches extending out from the larger vessels, which was not evident across similar-sized vessels in DM control mice. Both the scar-like accumulation around larger vessels and the reactive processes extending along adjoining capillaries were closely associated with morphologically restricted albumin staining in tight proximity with the vasculature. In comparison, the MWCNT-induced dense recruitment of activated microglia appeared to be broadly arrayed around larger vessels, with no specific morphological association to the endothelial wall or capillary branches (IBA1 staining; Fig. 2*C*). However, arrayed microglial processes were significantly correlated with the extravascular albumin halo found to surround the larger vessels of mice exposed to 10 μg ($r_p = 0.6$; $r_s = 0.62$; $P < 0.0001$) or 40 μg ($r_p = 0.58$; $r_s = 0.63$; $P < 0.0001$) MWCNTs, which was otherwise absent in DM control animals. Two-dimensional histograms showing albumin and glial markers emphasize the strong correlation ($r \geq 0.6$) of IBA1 staining selectively with the albumin halo (Fig. 2*D*), as opposed to GFAP staining, in which the majority of higher-intensity pixels were correlated with low-intensity albumin staining. However, a greater correlation between higher-intensity GFAP-stained pixels and higher-intensity albumin staining is seen in the 40 μg MWCNT dose ($r_p = 0.32$, $r_s = 0.44$; $P < 0.0001$) relative to the 10 μg MWCNT dose ($r_p = 0.18$, $r_s = 0.29$; $P < 0.0001$), indicative of the greater amount of albumin confined in close proximity to the vasculature by reactive glial processes. These data support the conclusion of a predominant colocalization between microglia and leaked albumin, consistent with the phagocytic functionality of these cells under neuroinflammatory conditions.

Dependence of MWCNT-Induced Neuroinflammation on BBB Disruption. To mechanistically delineate whether neuroinflammation was the result of BBB disruption, mice were administered vehicle or the rho kinase inhibitor fasudil, which has been shown to improve BBB function by relaxing cytoskeletal interactions in endothelial cells, thereby improving outcomes in stroke-related models (26, 27). Mice received fasudil either 2 h after MWCNT aspiration but before injection of the BBB tracer sodium fluorescein or just before MWCNT aspiration and again 2 h later (Fig. 3*A*). The former permutation was designed to test whether fluorescein uptake in the brain was inhibited after exposure and exposure-induced neuroinflammation had occurred. The latter permutation was implemented to prevent BBB disruption prophylactically and throughout the exposure to test whether neuroinflammatory changes still occurred in the absence of BBB disruption.

As was demonstrated microscopically (Fig. 1 *A* and *B*), fluorescein uptake in brain homogenates was significantly enhanced at 4 h after pulmonary exposure to MWCNTs (Fig. 3*B*). Increased *Il6* and *Ccl5* mRNA expression was induced by MWCNTs in cortical regions (Fig. 3*C*). Treatment with fasudil at 2 h postexposure completely blocked fluorescein uptake in the brain, but had no effect on neuroinflammatory outcomes (Fig. 3 *B* and *C*); however, prophylactically administered fasudil was

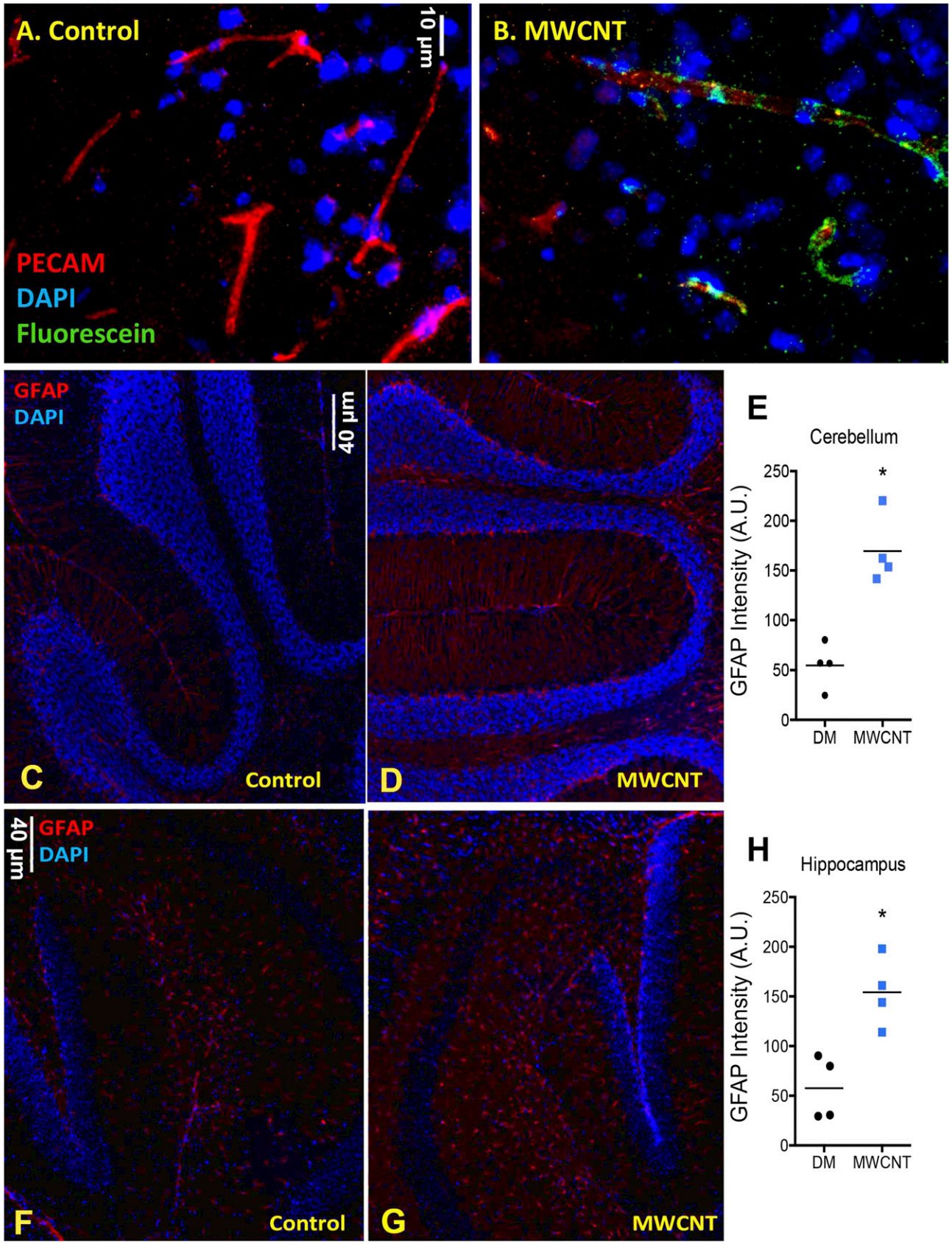

Fig. 1. MWCNT (10 μg) aspiration acutely reduces BBB integrity and induces GFAP expression on astrocytes. (*A* and *B*) Fluorescein staining (green) is not apparent in control-treated mouse brains (*A*), but is clearly adjacent to vascular structures (red; PECAM) in MWCNT-treated mice (*B*). (*C–H*) Enhanced GFAP staining (red) in the cerebellum (*C–E*) and hippocampus (*F–H*) of control and MWCNT-treated mice, indicative of astrocyte activation. *P <0.05, Student's *t* test.

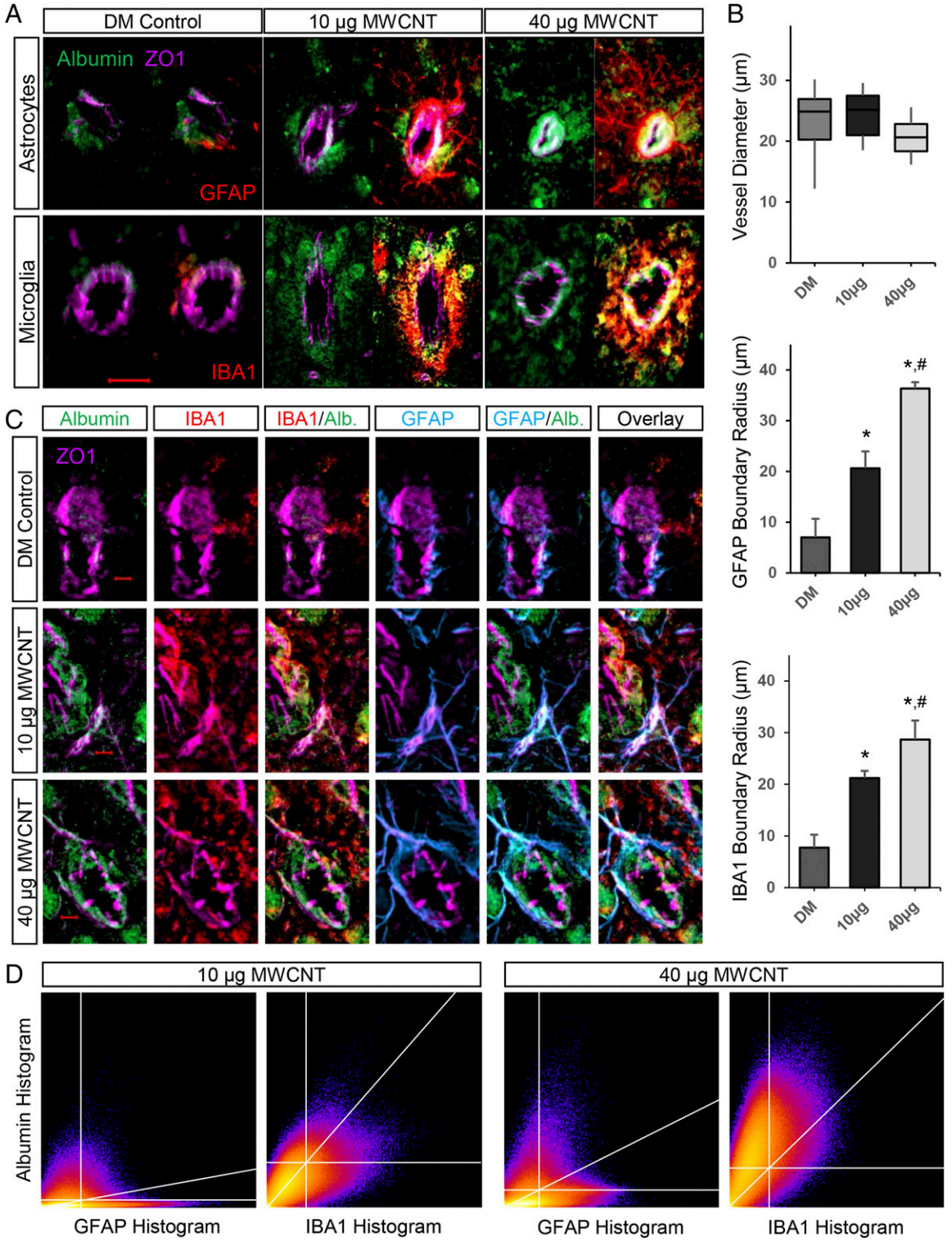

Fig. 2. MWCNT-induced BBB disruption promotes astrocytic and microglial reactivity selectively around larger cerebrovasculature. (*A*) Distinct extravascular accumulation of serum albumin (green) is observed following 10 μg and 40 μg MWCNT exposures relative to control-treated mouse brains in larger cerebral vessels (>10-μm diameter) stained for ZO1 (magenta). These vessels are further enveloped by a dense accumulation of astrocytes (GFAP-stained) and microglia (IBA1-stained) that are reactive to MWCNT exposure, distinct from basal glial associations with vessels in DM control mouse brains. (Magnification: 200×.) (Scale bar: 20 μm.) (*B*) Boxplot depicting the diameter distribution in the assessed vessels. Bar graphs show the boundary thickness for accumulated extravascular reactive glia extending out from the vessel wall (ZO1) in a dose-dependent manner. *$P < 0.05$ compared with DM control; #$P < 0.05$ compared with 10 μg MWCNT dose. (*C*) Optical sectioning (0.5-μm thickness) revealing a predominant colocalization of microglial (IBA1) staining encircling and engulfing leaked serum albumin, but astrocytes (GFAP) costaining with serum albumin only when in tight association with the vessel wall, indicative of the functional difference for the two glial responses. (Magnification: 400×.) (Scale bar: 5 μm.) (*D*) A 2D heatmap of results from colocalization analysis (Costes method), showing the correlation between albumin and either GFAP or IBA1 histogram pixel data. The upper right quadrant includes pixels demonstrating significant positive correlation between channels, the diagonal calculated linear regression line.

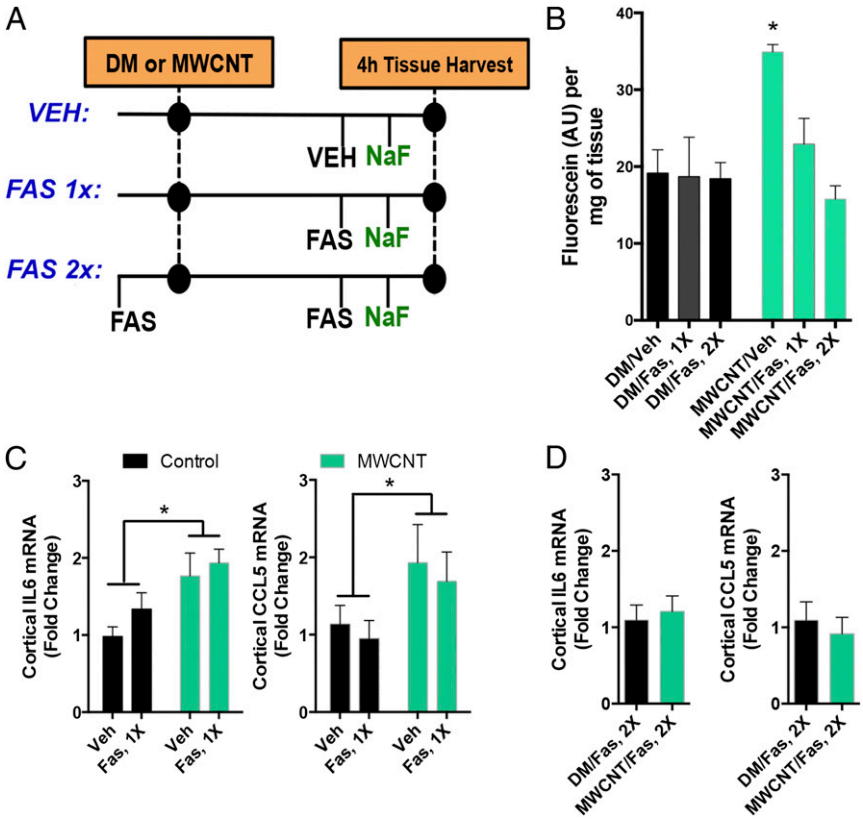

Fig. 3. MWCNT-induced neuroinflammatory responses are dependent on BBB disruption. (*A*) General study design, incorporating a single (1×) fasudil treatment after MWCNT to reduce brain fluorescein uptake and a preventative (2×) fasudil treatment to prevent MWCNT-induced BBB disruption throughout the 4-h time course. (*B*) Fluorescein uptake in brains at 4 h following MWCNT aspiration with vehicle, 1× fasudil, or 2× fasudil treatment. * $P < 0.05$ compared with control, ANOVA. (*C*) Inflammatory markers *Il6* and *Ccl5* mRNA in the cortex at 4 h after DM or MWCNT aspiration. *A significant effect of MWCNT compared with control in two-way ANOVA ($P < 0.05$) with no influence of the single post-MWCNT fasudil treatment. (*D*) Preventative (2×) fasudil administration abrogated inflammatory marker mRNA expression (*Il6*, *Ccl5*) in the cortex.

able to completely abrogate both fluorescein uptake (Fig. 3*B*) and neuroinflammatory outcomes (Fig. 3*D*), demonstrating that these neuroinflammatory responses depend on the loss of BBB integrity and penetration of circulating factors.

Bioactivity of MWCNT-Induced, Serum-Borne Factors: Endothelial Inflammatory Responses. We used cultured mouse cerebrovascular endothelial cells (mCECs) as biosensors of cumulative inflammatory mediators in serum from MWCNT-exposed mice, an approach that has proven valuable in toxicologic and clinical applications (16, 28). Microarray analysis was performed on mRNA isolated from primary mCECs following incubation with serum collected from MWCNT- or DM-exposed mice (at 4 h postexposure) at 10% in medium for 4 h (Fig. 4*A*). Microarray results revealed up-regulated genes associated with inflammation, immune response, and chemoattraction/recruitment of leukocytes (Figs. 4 *B* and *C* and Fig. S3). Importantly, the majority of up-regulated genes behaved in a dose-dependent manner, with more prominent effects seen in the 40 μg dose group (Table S1). Microarray findings were confirmed in subsequent assays, in which application of 10% serum from MWCNT-treated mice on primary mCECs for 4 h resulted in a 50% increase in relative mRNA expression of *Vcam1* and approximately threefold increases in relative mRNA expression of *Ccl2* and *Ccl5* proinflammatory cytokines in the 40 μg dose group at the 4 h timepoint (Fig. 4*D*).

Similarly, treatment of primary mCECs with serum from MWCNT-treated mice elicited a small but significant up-regulation of both vascular cell adhesion molecule 1 (VCAM-1) and intercellular adhesion molecule 1 (ICAM-1) protein on the cell surface, as assessed by flow cytometry (Fig. 4*E*). Serum obtained at 24 h postexposure exhibited lower inflammatory potency. These data, in conjunction with the gene expression findings, suggest that serum-induced increased mRNA expression translates into increased cell surface expression of protein, culminating in activation of the endothelium.

Bioactivity of MWCNT-Induced, Serum-Borne Factors: Endothelial Cell Regrowth and Motility. Whereas up-regulated genes (Fig. 4*B*, red) in serum-treated cells trended in a dose-dependent manner, down-regulated genes (Fig. 4*B*, blue) exhibited a biphasic response, in which effects were most potent at the 10 μg dose. Down-regulated genes aligned with categories of cell proliferation, mitosis, and cytokinesis (Fig. 4*B* and Fig. S3); thus, wound healing deficits were confirmed functionally by a "scratch" assay. Serum from control and MWCNT-treated mice was applied to confluent primary mCECs that had been "scratched" with a sterile pipette tip and allowed to grow back over 6 h. At the 6 h mark, the control serum-treated cells had achieved a mean distance of cell regrowth of 100 μm, compared with ∼60 μm of growth for the 40 μg dose group and only ∼50 μm of growth for the 10 μg dose group (Fig. 4 *F* and *G*). These results are congruent with the biphasic changes seen in the microarray results.

TSP-1 and CD36: Plausible Ligand–Receptor Interaction. The foregoing findings further suggest that endothelial cells interact with blood-borne factors generated by pulmonary MWCNT exposure. We have previously shown a role for the endothelial cell surface

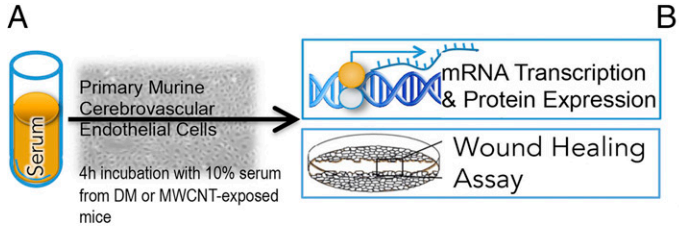

B

Upregulated Pathways

Gene Ontology	# Genes	P Value	Bayes Factor
Response to biotic stimulus	15	< 0.0001	20
Immune response	12	< 0.0001	15
Defense response	12	< 0.0001	14
Response to stimulus	15	< 0.0001	10
Inflammatory response	6	< 0.0001	10
Response to stress	10	< 0.0001	9
Response to wounding	6	< 0.0001	7
Response to pest/pathogen/parasite	7	< 0.0001	7

Downregulated Pathways

Gene Ontology	# Genes	P Value	Bayes Factor
Cell proliferation	18	< 0.0001	33
M Phase	11	< 0.0001	30
Cell Cycle	15	< 0.0001	28
Mitosis	9	< 0.0001	26
M Phase of Mitotic Cell Cycle	9	< 0.0001	26
Nuclear Division	9	< 0.0001	23
Mitotic Cell Cycle	9	< 0.0001	23
Cytokinesis	6	< 0.0001	20
Microtubule-based process	5	< 0.0001	20

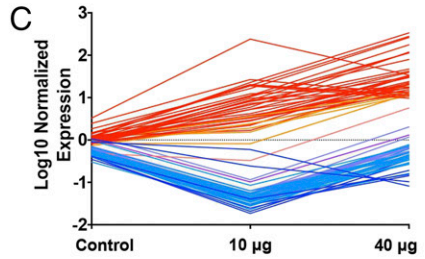

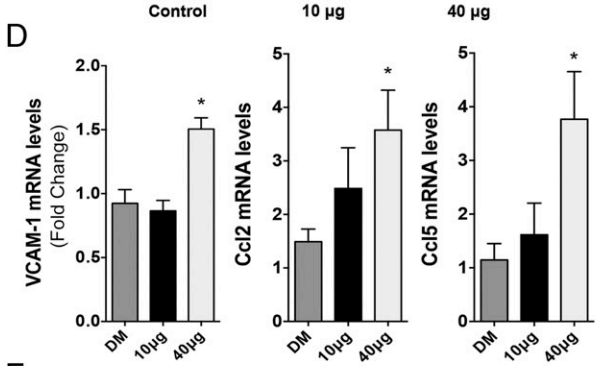

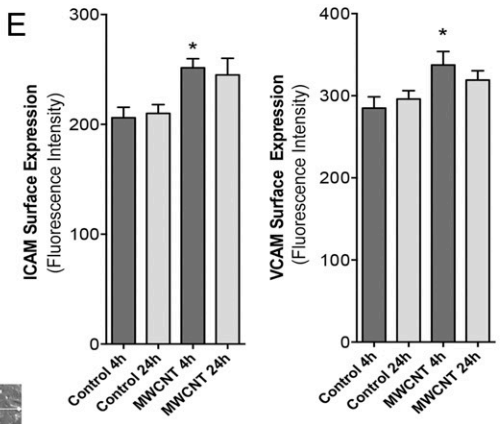

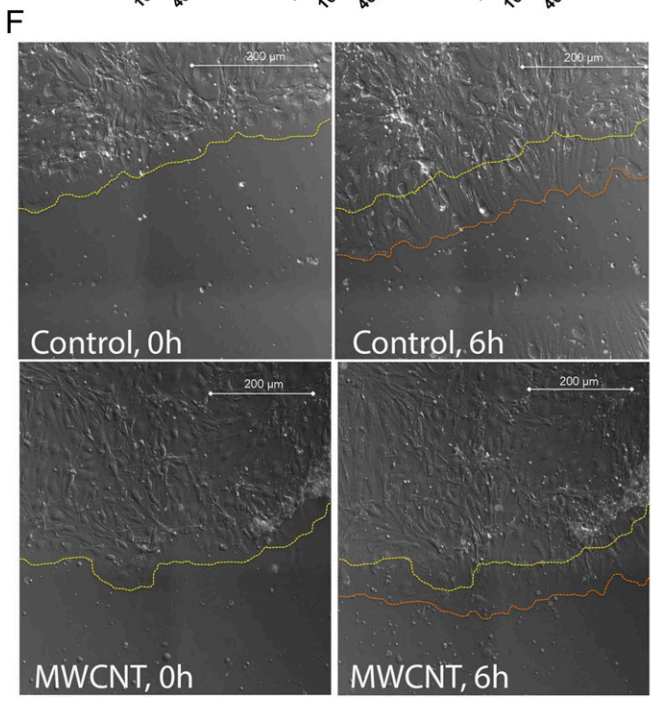

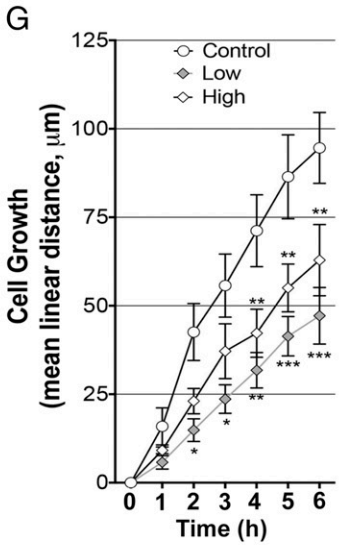

Fig. 4. Inflammatory responses of cerebrovascular endothelial cells treated with serum from MWCNT-exposed mice. (*A*) General depiction of inflammatory potential assay and wound healing protocols, with serum from exposed mice incubated on primary murine cerebrovascular endothelial cells. (*B*) Microarray results indicating numerous significantly altered transcripts ($n = 84$) from endothelial cells incubated with serum from MWCNT-exposed mice, compared with cells incubated with serum from control mice (at 4 h after aspiration). (*C*) Elevated transcripts (in red) were ontologically related to inflammatory and/or cellular defense response, whereas down-regulated transcripts (blue) were related to proliferation and migration pathways, listed in the table. (*D*) Confirmation of key inflammatory mRNA responses by PCR showing that endothelial *Vcam1*, *Ccl2*, and *Ccl5* mRNA were significantly up-regulated by serum from MWCNT-treated mice. (*E*) Endothelial cell surface Icam-1 and Vcam-1 protein expression was elevated by serum from mice exposed to the 40 µg dose of MWCNTs at 4 h compared with controls. $*P < 0.05$ compared with DM control serum. (*F*) Live cell images of wound recovery in mCECs treated with serum from control and 40 µg MWCNT-treated mice, showing the initial edge of endothelial cells (yellow dashed line) and the edge after 6 h (orange dashed line). (*G*) Mean cell regrowth following wounding in primary cerebrovascular endothelial cells incubated with serum from DM- and MWCNT-exposed mice. $*P < 0.05$; $**P < 0.01$; $***P < 0.001$ compared with DM control serum effects, two-way repeated-measures ANOVA.

protein cluster of differentiation 36 (CD36) as a mediator of vasodilatory impairment following pulmonary exposure to ozone (17). CD36 is a class II scavenger receptor involved in a wide range of processes, including fatty acid metabolism (29), heart disease, and atherosclerosis (30). The endogenous ligand for CD36, TSP-1 (31), was significantly elevated in serum at 4 h after aspiration of 10 μg of MWCNTs in WT mice (Fig. 5 *A* and *B*); however, the MWCNT activation of GFAP observed in WT mice was not observed in CD36$^{-/-}$ mice (Fig. 5*C*). Furthermore, CD36$^{-/-}$ mice exposed to MWCNTs showed no increases in cortical fluorescein uptake (Fig. 5*D*) or proinflammatory gene expression in the cortex (Fig. 5*E*) or hippocampus (Fig. 5*F*) compared with DM control mice, consistent with a role for scavenger receptor interaction with circulating ligands.

Discussion

Neurologic consequences of inhaled PM and gases have been reported in epidemiologic and toxicologic studies, but considerable uncertainty exists regarding the pathway by which toxic effects transfer from the lung to the brain (3, 32–34). The present study establishes that a circulating signal arises after pulmonary exposure to MWCNTs that leads to a BBB-dependent neuroinflammatory response. Serum from MWCNT-exposed mice upregulated adhesion molecules and proinflammatory cytokines in primary cerebrovascular endothelial cells at both the gene and protein level. Serum from exposed mice also adversely affected the ability of endothelial cells to migrate and recover in a wound-healing assay. TSP-1 was identified as a plausible serum-borne mediator of these effects, via interactions with CD36. Collectively, these outcomes implicate a modified serum composition stemming from pulmonary interactions with MWCNTs as a source of diminished BBB integrity and neural effects.

Inhalation of PM has been associated with BBB integrity deficits and neuroinflammation (23, 35), but this mechanistic study shows an interactive link between the two outcomes. Rats exposed to diesel emissions for 6 mo demonstrated significant increases in cortical TNFα, α-synuclein, and amyloid-β42 peptide expression (36). Oppenheim et al. (37) identified significant increases in brain fluorescein uptake resulting from long-term exposure (50 d) to a mixture of gasoline and diesel emissions in ApoE$^{-/-}$ mice. These findings were associated with increased cerebrovascular gelatinase levels and reduced occludin and claudin-5 expression and, in parallel, increased inducible nitric oxide synthase expression in the brain parenchyma. MWCNT aspiration induced a similar pattern of fluorescein uptake into the brain, whereas rho-kinase inhibition blocked this effect and, when administered prophylactically, also prevented neuroinflammatory responses. Fasudil likely does not alter the pathways leading to occluding and claudin-5 down-regulation, but rather relaxes intracellular endothelial cytosketetal components to shift the force balance from intercellular to intracellular, thereby reducing intercellular gap formation (38).

Our present findings suggest a focused but likely transient reduction in BBB integrity following a single exposure to MWCNTs. Broadly speaking, cerebral capillaries appear to be limited to small-molecule BBB permeation, as demonstrated by fluorescein uptake; however, the larger-diameter vessels and immediate branches that feed the microvasculature sustain greater BBB disruption, as evidenced by dose-dependent albumin protein leakage. Larger arterioles may be more susceptible owing to their higher perfusion pressure, leaving the adjacent neuropils highly vulnerable to MWCNT-induced neuroinflammation. Capillary- and arteriole-associated BBB permeations, along with molecular evidence, were observed across functionally disparate cortical, hippocampal, thalamic, and cerebellar regions, indicating a global rather than a domain-specific cerebrovascular response. However, regional susceptibility remains, likely owing to activity-dependent variations in cerebrovascular density (39), with functional implications to be addressed in follow-up studies. Reactive astrocytes effectively confined capillary leakage in close proximity to the

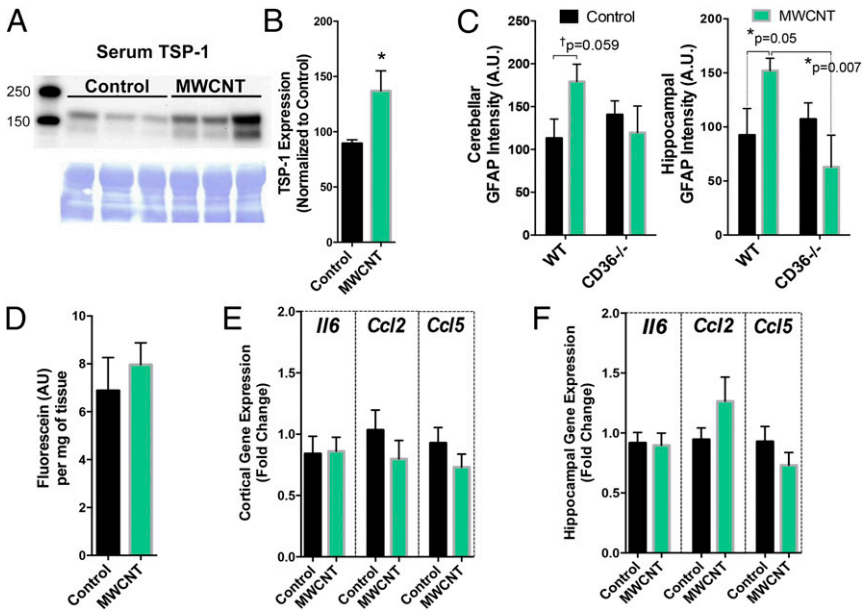

Fig. 5. Serum TSP-1 levels are increased by MWCNT treatment, and CD36 mice are largely protected from the BBB disruption and neuroinflammatory effects of pulmonary MWCNT exposure. (*A*) TSP-1 protein levels in serum from control (left three lanes) and MWCNT-treated mice (right three lanes) normalized to Coomassie blue loading controls. (*B*) Quantification of TSP-1 protein levels from all study subjects. $n = 5–6$. *$P < 0.05$, Student's *t* test. (*C*) GFAP staining in WT and CD36$^{-/-}$ mice treated with MWCNTs. Cortex (*Left*) and hippocampus (*Right*) were imaged as described for Fig. 1. WT mice displayed similar findings as shown previously, whereas CD36$^{-/-}$ mice showed no impact of MWCNT exposure on GFAP staining intensity. *$P < 0.05$, two-way ANOVA with Fisher's least significant difference post hoc comparison test. (*D*) Fluorescein uptake in the brain of CD36$^{-/-}$ mice at 4 h after treatment with vehicle (DM) or MWCNTs. (*E* and *F*) Neuroinflammatory mRNA markers in the cortex (*E*) and hippocampus (*F*) of control and MWCNT-treated CD36$^{-/-}$ mice.

vessel; however, the emergence of an astroglial scar-like formation around larger vessels, likely to limit prolonged leakage around larger vessels, appeared to be transiently ineffective in confining the initial BBB leakage. Permeation of the BBB beyond an astrocytically confined limit also promoted dose-dependent microglial activation and recruitment around larger vessels. Correlated with the halo of leaked serum components, phagocytic microglia provided the means to clean up after acute BBB permeation (40). Future studies are needed to assess the duration of microglial activation in and around larger vessels and to investigate whether chronic MWCNT exposure may promote a worsened proinflammatory phenotype (41).

Disruption of BBB integrity has been documented in major cerebrovascular events or neurologic diseases, and BBB permeability can be tied to neuroinflammation. Mouse models of Alzheimer's disease have found that BBB permeability precedes the formation of the β-amyloid plaques that are the hallmark of the disease (42). Following MWCNT exposure, BBB disruption led to neuroinflammation, which was effectively blocked with the prophylactic application of the rho-kinase inhibitor fasudil. Rho-kinase inhibition has been shown to reduce neuropathology in scenarios in which BBB is otherwise dysfunctional. Fasudil treatment in a mouse ischemia model was found to prevent BBB permeability, as well as the formation of oxidative stress (27). Rho-kinase inhibition with fasudil also has been shown to accelerate functional recovery in spinal cord injury models (43, 44). Autoimmune demyelinating disorders, such as multiple sclerosis, have been treated with rho-kinase inhibitors with great success; it is thought that rho-kinase inhibition in these disorders prevents leukocyte migration into the central nervous system (45). Fasudil inhibited fluorescein uptake into the brain regardless of the time of injection, but did not inhibit neuroinflammation when given after MWCNT administration, which indicates a potential for circulating factors arising from the lung to trigger a loss of BBB integrity. Moreover, the improvement in BBB integrity with no impact on neuroinflammatory responses seen when fasudil was administered after MWCNTs indicates that the principal target of fasudil is the vascular endothelium.

We have previously demonstrated that serum derived from ozone-exposed mice diminishes vasodilatory responses through the class B scavenger receptor CD36 (17); thus, we tested whether CD36 and its endogenous ligand, TSP-1, may have a role in the BBB alterations caused by MWCNTs. CD36 is expressed in the rodent cerebrovasculature (46) and, interestingly, appears to be present in larger cerebral vessel endothelium (where substantial serum albumin leakage is seen) and in pericytes in humans (47), but may be less relevant in the microvasculature, although still expressed at low levels (48). Vascular CD36 mediates free radical production and brain injury in cerebral ischemia (46) and also has been shown to activate the rho/rho-kinase pathway (49). In the present study, serum TSP-1 level was elevated by MWCNT aspiration, and the absence of CD36 prevented both the increased BBB permeability and neuroinflammation induced by MWCNT exposure. Importantly, previous studies with related pollutants have noted the involvement of related scavenger receptors (including CD36, Toll-like receptor 4, and lectin-like receptor for oxidized low-density lipoprotein 1) and ligands (including oxidized lipids and lipoproteins) (17, 50). Thus, TSP-1 is likely an important facet of a more complex response to inhaled agents, and further studies are needed to identify the origin of TSP-1 and the timing of the response, to mechanistically confirm the interaction with CD36 and/or CD47 on endothelial cells, and to ascertain whether TSP-1 specifically crosses into the brain.

Alternate pathways for the neural effects of inhaled PM, such as direct delivery of inhaled particulates to the brain or other target organs, have been hypothesized, but quantitative evidence demonstrating substantive transference of CNTs across the BBB are limited (12) and, more crucially, no evidence of a direct biological effect has been mechanistically established. Specifically, MWCNTs accumulate in the brain at only small fractions of the original pulmonary dosage (0.00022% of the lung burden following a 12-d exposure), and specific confirmation that the material has penetrated beyond the capillary wall is often lacking in distribution studies; that is, much of the residual mass of MWCNTs may simply reside in the cerebrovascular compartment and not in brain tissue (12). Even when specifically engineering nanoparticles to access the brain, researchers find it exceedingly difficult to overcome the BBB (51, 52). An important factor in the interpretation of our present findings is the short time course (4 h), which is likely too short for significant translocation of MWCNTs beyond the lung; however, longer-term outcomes may arise as a result of either continued pulmonary interactions or direct access and accumulation in the brain.

A broader impact of pulmonary inflammation on neurologic outcomes is implied by our findings, which may explain more generally the comorbid associations between lung disease and cognition deficits and neurodegenerative diseases (53, 54). A loss of BBB integrity caused by circulating factors of pulmonary origin may be central to the neurologic outcomes of pulmonary inflammation, remodeling, or toxicity owing to inhaled toxicants. Given the suggestive adjuvant role for inhaled PM in driving neurodevelopmental and neurodegenerative diseases (1, 2), factors such as TSP-1 may explain in part how indirect pulmonary responses can exacerbate neurologic diseases. A more thorough characterization of circulatory molecular changes after MWCNT exposure is warranted, given the vast number of potential alterations to endogenous components.

Materials and Methods

The study design, assays, and statistical analysis are described in detail in *SI Materials and Methods*. All procedures involving vertebrate animals were approved by the Animal Care and Use Committees of the University of New Mexico and the National Institute of Occupational Safety and Health.

ACKNOWLEDGMENTS. A.E. thanks Diane Schwegler-Berry for the electron microscopy images of the MWCNT. Microarray analyses were conducted in the KUGR Genomics Facility at University of New Mexico with valuable support from Gavin Pickett. Dr. Michael Paffett supported a portion of the immunohistochemical image generation and analysis through the University of New Mexico and Cancer Center Fluorescence Microscopy Shared Resource, funded as detailed at hsc.unm.edu/crtc/microscopy/acknowledgement.shtml. The antibody to ZO1 (R26.4C) was developed by D. A. Goodenough at Harvard Medical School and was obtained from the Developmental Studies Hybridoma Bank, created by the Eunice Kennedy Shriver National Institute of Child Health and Human Development NICHD and maintained at the University of Iowa. This study was funded by grants from the National Institute for Occupational Safety and Health [010828 (to M.J.C.), 010495 (to M.J.C. and A.K.O.), and NTRC 939ZXFL (to A.E.)] and the National Institutes of Health [ES014639 (to M.J.C.), ES023060 (to A.K.O.), GM088021 (to K.Z.), and HL007736 (to M.J.A.)]. The findings and conclusions in this report are those of the authors and do not necessarily represent the views of the National Institutes of Health and the National Institute for Occupational Safety and Health.

1. Kioumourtzoglou MA, et al. (2016) Long-term $PM_{2.5}$ exposure and neurological hospital admissions in the northeastern United States. *Environ Health Perspect* 124(1): 23–29.
2. Loane C, Pilinis C, Lekkas TD, Politis M (2013) Ambient particulate matter and its potential neurological consequences. *Rev Neurosci* 24(3):323–335.
3. Volk HE, Hertz-Picciotto I, Delwiche L, Lurmann F, McConnell R (2011) Residential proximity to freeways and autism in the CHARGE study. *Environ Health Perspect* 119(6):873–877.
4. Kafa H, et al. (2015) The interaction of carbon nanotubes with an in vitro blood-brain barrier model and mouse brain in vivo. *Biomaterials* 53:437–452.
5. De Pittà M, Brunel N, Volterra A (2016) Astrocytes: Orchestrating synaptic plasticity? *Neuroscience* 323:43–61.
6. Lou N, et al. (2016) Purinergic receptor P2RY12-dependent microglial closure of the injured blood-brain barrier. *Proc Natl Acad Sci USA* 113(4):1074–1079.
7. Salter MW, Beggs S (2014) Sublime microglia: Expanding roles for the guardians of the CNS. *Cell* 158(1):15–24.

8. Ormsby RW, Modreanu M, Mitchell CA, Dunne NJ (2014) Carboxyl functionalised MWCNT/polymethyl methacrylate bone cement for orthopaedic applications. *J Biomater Appl* 29(2):209–221.
9. Hamilton RF, Jr, Wu Z, Mitra S, Shaw PK, Holian A (2013) Effect of MWCNT size, carboxylation, and purification on in vitro and in vivo toxicity, inflammation and lung pathology. *Part Fibre Toxicol* 10(1):57.
10. Mercer RR, et al. (2011) Pulmonary fibrotic response to aspiration of multi-walled carbon nanotubes. *Part Fibre Toxicol* 8:21.
11. Ryman-Rasmussen JP, et al. (2009) Inhaled multiwalled carbon nanotubes potentiate airway fibrosis in murine allergic asthma. *Am J Respir Cell Mol Biol* 40(3):349–358.
12. Mercer RR, et al. (2013) Extrapulmonary transport of MWCNT following inhalation exposure. *Part Fibre Toxicol* 10:38.
13. Erdely A, et al. (2009) Cross-talk between lung and systemic circulation during carbon nanotube respiratory exposure: Potential biomarkers. *Nano Lett* 9(1):36–43.
14. Erdely A, et al. (2011) Identification of systemic markers from a pulmonary carbon nanotube exposure. *J Occup Environ Med* 53(6 Suppl):S80–86.
15. Aragon M, et al. (2016) MMP-9-dependent serum-borne bioactivity caused by multiwalled carbon nanotube exposure induces vascular dysfunction via the CD36 scavenger receptor. *Toxicol Sci* 150(2):488–498.
16. Channell MM, Paffett ML, Devlin RB, Madden MC, Campen MJ (2012) Circulating factors induce coronary endothelial cell activation following exposure to inhaled diesel exhaust and nitrogen dioxide in humans: Evidence from a novel translational in vitro model. *Toxicol Sci* 127(1):179–186.
17. Robertson S, et al. (2013) CD36 mediates endothelial dysfunction downstream of circulating factors induced by O_3 exposure. *Toxicol Sci* 134(2):304–311.
18. Harrison DG (1994) Endothelial dysfunction in atherosclerosis. *Basic Res Cardiol* 89 (Suppl 1):87–102.
19. Takeda S, Sato N, Morishita R (2014) Systemic inflammation, blood-brain barrier vulnerability and cognitive/non-cognitive symptoms in Alzheimer disease: Relevance to pathogenesis and therapy. *Front Aging Neurosci* 6:171.
20. Sweeney MD, Ayyadurai S, Zlokovic BV (2016) Pericytes of the neurovascular unit: Key functions and signaling pathways. *Nat Neurosci* 19(6):771–783.
21. Bussy C, et al. (2015) Microglia determine brain region-specific neurotoxic responses to chemically functionalized carbon nanotubes. *ACS Nano* 9(8):7815–7830.
22. Lund AK, et al. (2009) Vehicular emissions induce vascular MMP-9 expression and activity associated with endothelin-1–mediated pathways. *Arterioscler Thromb Vasc Biol* 29(4):511–517.
23. Gerlofs-Nijland ME, et al. (2010) Effect of prolonged exposure to diesel engine exhaust on proinflammatory markers in different regions of the rat brain. *Part Fibre Toxicol* 7:12.
24. Levesque S, et al. (2011) Diesel exhaust activates and primes microglia: Air pollution, neuroinflammation, and regulation of dopaminergic neurotoxicity. *Environ Health Perspect* 119(8):1149–1155.
25. Porter DW, et al. (2010) Mouse pulmonary dose and time course responses induced by exposure to multi-walled carbon nanotubes. *Toxicology* 269(2-3):136–147.
26. Satoh S, et al. (1996) Neuroprotective properties of a protein kinase inhibitor against ischaemia-induced neuronal damage in rats and gerbils. *Br J Pharmacol* 118(7): 1592–1596.
27. Gibson CL, Srivastava K, Sprigg N, Bath PM, Bayraktutan U (2014) Inhibition of Rho-kinase protects cerebral barrier from ischaemia-evoked injury through modulations of endothelial cell oxidative stress and tight junctions. *J Neurochem* 129(5):816–826.
28. Agarwal B, et al. (2013) Resveratrol for primary prevention of atherosclerosis: Clinical trial evidence for improved gene expression in vascular endothelium. *Int J Cardiol* 166(1):246–248.
29. Hajri T, Han XX, Bonen A, Abumrad NA (2002) Defective fatty acid uptake modulates insulin responsiveness and metabolic responses to diet in CD36-null mice. *J Clin Invest* 109(10):1381–1389.
30. Febbraio M, et al. (2000) Targeted disruption of the class B scavenger receptor CD36 protects against atherosclerotic lesion development in mice. *J Clin Invest* 105(8): 1049–1056.
31. Silverstein RL, Febbraio M (2009) CD36, a scavenger receptor involved in immunity, metabolism, angiogenesis, and behavior. *Sci Signal* 2(72):re3.
32. Campbell A, et al. (2005) Particulate matter in polluted air may increase biomarkers of inflammation in mouse brain. *Neurotoxicology* 26(1):133–140.
33. Cheng H, et al. (2016) Nanoscale particulate matter from urban traffic rapidly induces oxidative stress and inflammation in olfactory epithelium with concomitant effects on brain. *Environ Health Perspect* 124(10):1537–1546.
34. Mumaw CL, et al. (2016) Microglial priming through the lung-brain axis: The role of air pollution-induced circulating factors. *FASEB J* 30(5):1880–1891.
35. Campbell A, Araujo JA, Li H, Sioutas C, Kleinman M (2009) Particulate matter-induced enhancement of inflammatory markers in the brains of apolipoprotein E knockout mice. *J Nanosci Nanotechnol* 9(8):5099–5104.
36. Levesque S, Surace MJ, McDonald J, Block ML (2011) Air pollution and the brain: Subchronic diesel exhaust exposure causes neuroinflammation and elevates early markers of neurodegenerative disease. *J Neuroinflammation* 8:105.
37. Oppenheim HA, et al. (2013) Exposure to vehicle emissions results in altered blood-brain barrier permeability and expression of matrix metalloproteinases and tight junction proteins in mice. *Part Fibre Toxicol* 10:62.
38. Baumer Y, Spindler V, Werthmann RC, Bünemann M, Waschke J (2009) Role of Rac 1 and cAMP in endothelial barrier stabilization and thrombin-induced barrier breakdown. *J Cell Physiol* 220(3):716–726.
39. Klein B, Kuschinsky W, Schröck H, Vetterlein F (1986) Interdependency of local capillary density, blood flow, and metabolism in rat brains. *Am J Physiol* 251(6 Pt 2): H1333–H1340.
40. Nimmerjahn A, Kirchhoff F, Helmchen F (2005) Resting microglial cells are highly dynamic surveillants of brain parenchyma in vivo. *Science* 308(5726):1314–1318.
41. Block ML (2014) Neuroinflammation: Modulating mighty microglia. *Nat Chem Biol* 10(12):988–989.
42. Ujiie M, Dickstein DL, Carlow DA, Jefferies WA (2003) Blood-brain barrier permeability precedes senile plaque formation in an Alzheimer's disease model. *Microcirculation* 10(6):463–470.
43. Dergham P, et al. (2002) Rho signaling pathway targeted to promote spinal cord repair. *J Neurosci* 22(15):6570–6577.
44. Fournier AE, Takizawa BT, Strittmatter SM (2003) Rho kinase inhibition enhances axonal regeneration in the injured CNS. *J Neurosci* 23(4):1416–1423.
45. Walters CE, et al. (2002) Inhibition of Rho GTPases with protein prenyltransferase inhibitors prevents leukocyte recruitment to the central nervous system and attenuates clinical signs of disease in an animal model of multiple sclerosis. *J Immunol* 168(8):4087–4094.
46. Ueno M, et al. (2011) The expression of CD36 in vessels with blood-brain barrier impairment in a stroke-prone hypertensive model. *Neuropathol Appl Neurobiol* 37(7): 727–737.
47. Rustenhoven J, et al. (2016) TGF-beta1 regulates human brain pericyte inflammatory processes involved in neurovasculature function. *J Neuroinflammation* 13:37.
48. Mitchell RW, On NH, Del Bigio MR, Miller DW, Hatch GM (2011) Fatty acid transport protein expression in human brain and potential role in fatty acid transport across human brain microvessel endothelial cells. *J Neurochem* 117(4):735–746.
49. Wraith KS, et al. (2013) Oxidized low-density lipoproteins induce rapid platelet activation and shape change through tyrosine kinase and Rho kinase-signaling pathways. *Blood* 122(4):580–589.
50. Kampfrath T, et al. (2011) Chronic fine particulate matter exposure induces systemic vascular dysfunction via NADPH oxidase and TLR4 pathways. *Circ Res* 108(6):716–726.
51. Ren J, et al. (2012) The targeted delivery of anticancer drugs to brain glioma by PE-Gylated oxidized multi-walled carbon nanotubes modified with angiopep-2. *Biomaterials* 33(11):3324–3333.
52. Kateb B, et al. (2007) Internalization of MWCNTs by microglia: Possible application in immunotherapy of brain tumors. *Neuroimage* 37(Suppl 1):S9–S17.
53. Bu XL, et al. (2015) Serum amyloid-beta levels are increased in patients with chronic obstructive pulmonary disease. *Neurotox Res* 28(4):346–351.
54. Habeych ME, Castilla-Puentes R (2015) Comorbid medical conditions in vascular dementia: A matched case-control study. *J Nerv Ment Dis* 203(8):604–608.
55. Porter DW, et al. (2013) Acute pulmonary dose-responses to inhaled multi-walled carbon nanotubes. *Nanotoxicology* 7(7):1179–1194.
56. Topper LA, Baculis BC, Valenzuela CF (2015) Exposure of neonatal rats to alcohol has differential effects on neuroinflammation and neuronal survival in the cerebellum and hippocampus. *J Neuroinflammation* 12:160.
57. Schindelin J, et al. (2012) Fiji: An open-source platform for biological-image analysis. *Nat Methods* 9(7):676–682.
58. Costes SV, et al. (2004) Automatic and quantitative measurement of protein-protein colocalization in live cells. *Biophys J* 86(6):3993–4003.
59. Livak KJ, Schmittgen TD (2001) Analysis of relative gene expression data using real-time quantitative PCR and the 2(-delta delta C(T)) method. *Methods* 25(4):402–408.
60. Erdely A, et al. (2014) Oxidative stress and reduced responsiveness of challenged circulating leukocytes following pulmonary instillation of metal-rich particulate matter in rats. *Part Fibre Toxicol* 11:34.